

# Non-blocking $2 \times 2$ switching unit based on nested silicon microring resonators with high extinction ratios and low crosstalks

Jiayang Wu · Xinhong Jiang · Ting Pan ·  
Pan Cao · Liang Zhang · Xiaofeng Hu ·  
Yikai Su

Received: 1 December 2013 / Accepted: 20 March 2014 / Published online: 27 May 2014  
© Science China Press and Springer-Verlag Berlin Heidelberg 2014

**Abstract** In this paper, we propose and demonstrate a  $2 \times 2$  optical Benes switching unit based on two nested silicon microring resonators (MRRs) monolithically integrated on a silicon-on-insulator (SOI) wafer. High extinction ratios (ERs) of about 44.7/38.0 dB and low crosstalk values of about  $-37.5/-45.2$  dB at cross/bar states are obtained with the fabricated device. The operation principle is theoretically studied and the switching function is verified by system demonstration experiments with 10 and 12.5 Gb/s non-return-to-zero (NRZ) signals. The switching speed on the order of gigahertz based on free carrier effect in silicon is also experimentally demonstrated.

**Keywords** Optical switching unit · Microring resonator · High extinction ratio · Low crosstalk

## 1 Introduction

After decades of development, electrical interconnects based on metal lines are rapidly approaching their fundamental speed limitations [1, 2], which hinder further improvement of conventional chip multi-processors (CMPs). In comparison with the electrical counterparts, optical interconnects based on photonic devices are advantageous in high-speed processing due to wider bandwidth, lower latency, and lower power consumption [3–5]. Moreover, recent advances in the

fabrication of silicon photonic devices using the standard complementary metal-oxide-semiconductor (CMOS) processes provide sufficient integration density and enable the development of high-capacity optical network-on-chips (NoCs) [6–8]. Many functional building blocks to construct the optical NoCs have been proposed and experimentally demonstrated, such as switches [9], filters [10], modulators [11], and detectors [12].

Switching node, which performs the function of selecting the paths between a set of input and output ports, is a key element in optical NoCs. Owing to the compact footprint, CMOS compatibility, and potential sub-nanosecond switching time, silicon microring resonators (MRRs) are promising for the implementation of large-scale-integrated optical switching nodes [13, 14]. Some schemes of  $2 \times 2$  optical switching unit based on silicon MRRs have been studied in previous reports [14–17]. But the extinction ratio (ER) of a certain output port and crosstalk between different output ports remain severe problems to solve towards constructing high-performance switching units and improving the scalability of MRRs-based optical interconnections. To deal with these problems, we propose a new  $2 \times 2$  non-blocking Benes switching unit implemented by two nested silicon MRRs in this paper. Compared with the  $2 \times 2$  Benes switching units in [14] and [15], the performances of ER and crosstalk are significantly improved without introducing more MRRs. High extinction ratios (ERs) of about 44.7/38.0 dB and low crosstalk values of about  $-37.5/-45.2$  dB at cross/bar states are achieved with the fabricated device. The operation principle is theoretically analyzed and system experiments with 10 and 12.5 Gb/s NRZ signals are performed to verify the switching function. The switching time on the order of nanosecond based on silicon free carrier effect is also experimentally demonstrated.

SPECIAL TOPIC: All-Optical Signal Processing

J. Wu · X. Jiang · T. Pan · P. Cao · L. Zhang ·  
X. Hu · Y. Su (✉)

State Key Laboratory of Advanced Optical Communication  
Systems and Networks, Department of Electronic Engineering,  
Shanghai Jiao Tong University, Shanghai 200240, China  
e-mail: yikaisu@sjtu.edu.cn

## 2 Device structure and operation principle

Figure 1a illustrates the schematic diagram of the proposed  $2 \times 2$  switching unit consisting of two symmetric nested MRRs [18]. The bottom parts of the U-bend waveguides in the two nested MRRs are coupled with each other, which form a central directional coupler. There are four ports in the proposed switching unit, namely  $IN_1$ ,  $IN_2$ ,  $OUT_1$ , and  $OUT_2$ , as shown in Fig. 1a. Benes switching architecture is selected since it exhibits minimum complexity among various non-blocking switching architectures [14].

By using the scattering matrix method [19], we obtain the normalized transmission spectra from  $IN_1$  to  $OUT_2$  and  $OUT_1$ , as shown in Fig. 2a and b, respectively. Similar to single nested MRR in [18], the structural parameters are chosen as follows: the gap size is  $0.18 \mu\text{m}$ , the coupling lengths are  $L_{c1} = L_{c2} = 7 \mu\text{m}$ , the cross sections of the waveguides are  $450 \text{ nm} \times 220 \text{ nm}$ , the ring radius is  $R_2 = 40 \mu\text{m}$ , and the straight part of the U-bent waveguide is  $L = 128 \mu\text{m}$ . The transmission coefficients of the directional couplers calculated by using Lumerical finite-difference time-domain (FDTD) solutions are  $r_1 = r_2 = 0.8250$ . Based on our previously fabricated devices, the waveguide group index of the transverse electric (TE) mode and the waveguide loss factor are assumed to be  $n_g = 4.3350$  and  $\alpha = 350 \text{ m}^{-1}$ , respectively. The resonance notch depths in Fig. 2a and b, i.e., the ERs of the switching unit, are further increased in comparison with those of a single nested MRR,

since the input light goes through the two symmetric nested MRRs with the same resonances. Figure 2c illustrates the normalized spectrum of  $T_{11}/T_{12}$ , where  $T_{11}$  and  $T_{12}$  are the transmission spectra in Fig. 2a and b, respectively. In Fig. 2c, there are peaks and notches at the resonance wavelengths in Fig. 2a and b with different heights and depths corresponding to various crosstalk values of the switching unit. The peaks and notches possess a periodic envelop covering several free spectral ranges (FSRs), and one can always find a condition with a minimum crosstalk value in an envelope period. Furthermore, the minimum crosstalk value of the switching unit can be further optimized by finely tuning the phase shift along  $L$ . In Fig. 2d, we plot zoom-in view of Fig. 2a and b in the wavelength range of  $1549.5\text{--}1551.5 \text{ nm}$ . The proposed switching unit operates in the cross state at the wavelength of  $w_1$  with a crosstalk value of about  $-48 \text{ dB}$ . On the other hand, it operates in the bar state at the wavelength of  $w_2$  with a crosstalk value of about  $-47 \text{ dB}$ .

## 3 Device fabrication and measured spectra

The designed device based on the above principle is fabricated on an 8-inch silicon-on-insulator (SOI) wafer with a 220-nm-thick top silicon layer and a 2- $\mu\text{m}$ -thick buried dioxide (BOX) layer. The micrograph showing the fabricated device as well as the scanning electron microscope

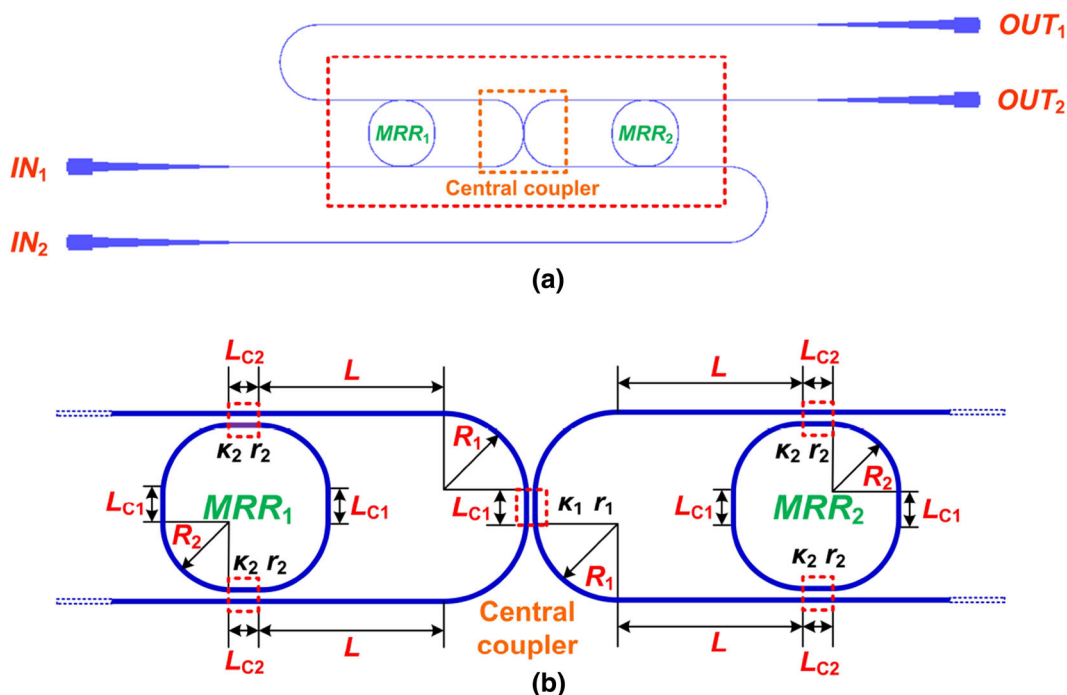


**Fig. 1** (Color online) Device configuration. **a** Schematic diagram of the proposed  $2 \times 2$  switching unit based on two nested silicon MRRs; **b** Zoom-in view of the dashed box in **a**. MRR microring resonator

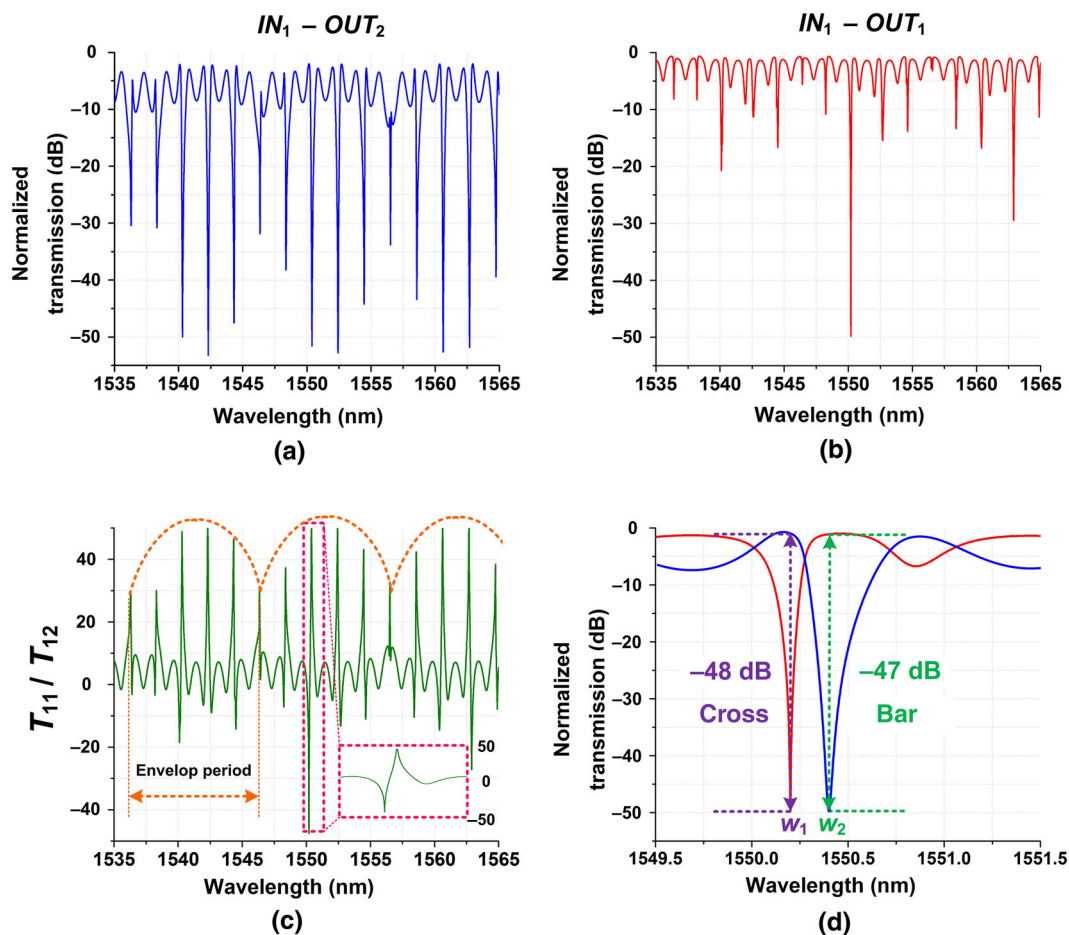


**Fig. 2** (Color online) Transmission spectra of the proposed device calculated by using the scattering matrix method. **a** Normalized transmission spectrum from  $IN_1$  to  $OUT_2$  ( $T_{12}$ ); **b** Normalized transmission spectrum from  $IN_1$  to  $OUT_1$  ( $T_{11}$ ); **c** Normalized spectrum of  $T_{11}/T_{12}$ , zoom-in view in the wavelength range of 1549.5–1551.5 nm is shown in the inset; **d** Zoom-in view of (a) and (b) in the wavelength range of 1549.5–1551.5 nm,  $w_1$  and  $w_2$  denote the two resonance wavelengths in (d)

(SEM) photos of the central directional coupler and  $MRR_2$  are presented in Fig. 3a. 248-nm deep ultraviolet (DUV) photolithography is utilized to define the pattern and an inductively coupled plasma (ICP) etching process is used to etch the top silicon layer. Grating couplers for TE polarization are employed at the end of input/output ports to couple light into and out of the chip with single-mode fibers (SMFs). Thermal-optic microheater is fabricated along  $MRR_1$  to make sure that there are identical resonance wavelengths of the two MRRs.

The normalized transmission spectra from  $IN_2$  to  $OUT_1$  and  $OUT_2$  measured with the fabricated device are shown in Fig. 3b by the solid curves. The on-chip insertion loss is about 11 dB. The measured curves are then fitted by the dashed curves calculated by using the scattering matrix method. The fitting parameters are  $r_1 = r_2 \approx 0.827$ ,  $\alpha \approx 390 \text{ m}^{-1}$ , and  $n_g \approx 4.2380$ . One can see from Fig. 3b that the experimentally measured curves fit well with the calculated curves. The measured transmission spectra from  $IN_1$  to  $OUT_2$  and  $OUT_1$

are shown in Fig. 3c. A thermal-optic micro-heater is employed to slightly shift the resonance wavelengths of  $MRR_1$  to make sure that  $\lambda_1 = \lambda_1' = 1551.282 \text{ nm}$  and  $\lambda_2 = \lambda_2' = 1551.516 \text{ nm}$ , where  $\lambda_{1,2}$  and  $\lambda_{1',2}'$  are the resonance wavelengths labeled in Fig. 3b and c, respectively.  $\lambda_1 = 1551.282 \text{ nm}$  and  $\lambda_2 = 1551.516 \text{ nm}$  are selected as the operation wavelengths of the cross state and bar state, respectively. The ERs and crosstalk values at  $\lambda_1$  and  $\lambda_2$  are shown in Table 1. The differences in ERs and crosstalk values between the cross and bar states are mainly attributed to the slight mismatch between the resonances of the MRR and that of the outer feedback loop in each nested MRR, which can be further reduced by finely tuning the phase shift along the U-bend waveguide. Similar to other silicon devices, the spectral response of the proposed device suffers from a thermal shift upon temperature variation. The temperature sensitivity can be reduced by overlaying a polymer cladding with negative thermal-optic coefficient on the devices to compensate the positive thermal-optic coefficient of silicon [20].

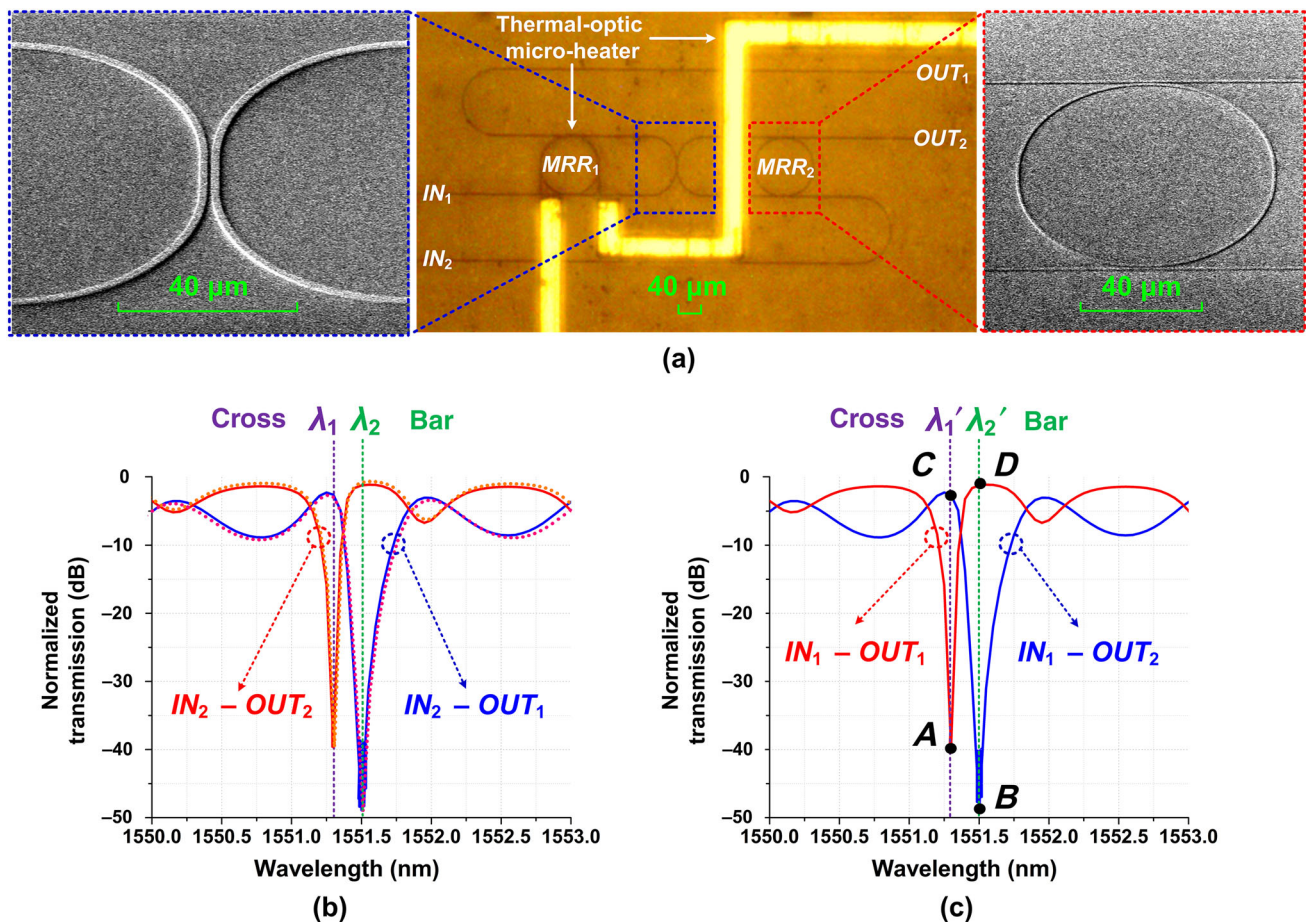


**Fig. 3** (Color online) Photos of the fabricated device and experimentally measured transmission spectra. **a** Micrograph of the fabricated device (middle) and SEM photos of the central directional coupler (left) and  $MRR_2$  (right); **b** Experimentally measured transmission spectra from  $IN_2$  to  $OUT_1$  and  $OUT_2$  (solid curves), theoretically fitted transmission spectra are correspondingly shown by dashed curves; **c** Experimentally measured transmission spectra from  $IN_1$  to  $OUT_2$  and  $OUT_1$ .  $\lambda_{1,2}$  and  $\lambda'_{1,2}$  denote resonance wavelengths in (b) and (c), respectively

**Table 1** Extinction ratios and crosstalk values of the fabricated device

Operation state	Cross	Bar
Operation wavelength (nm)	$\lambda_1 = \lambda'_1 = 1551.282$	$\lambda_2 = \lambda'_2 = 1551.516$
Extinction ratio (dB)	$P_C - P_B = 44.7$	$P_D - P_A = 38.0$
Crosstalk (dB)	$P_A - P_C = -37.5$	$P_B - P_D = -45.2$

$P_A$ ,  $P_B$ ,  $P_C$ , and  $P_D$  denote the transmission powers at point A, B, C, and D in Fig. 3c, respectively

#### 4 System demonstration of switching function

We use the experimental setup shown in Fig. 4 to test the performance of the fabricated device as a  $2 \times 2$  switching unit. The wavelength of the probe signal is set to  $\lambda_2 = 1551.516$  nm in Fig. 3b, and the wavelength of the pump light sits at another resonance wavelength of 1545.433 nm in the measured transmission spectrum from

$IN_1$  to  $OUT_2$ , as shown in Fig. 4. Due to the thermal nonlinear effect, a high-power input pump light at resonance wavelength of the device would induce red shift of the transmission spectra [21]. When  $\lambda_1 = 1551.282$  nm is red shifted to  $\lambda_2 = 1551.516$  nm, the switching unit changes from bar state to cross state. A Mach-Zehnder modulator (MZM) is driven by an electrical pseudo random bit sequence (PRBS) signal with a pattern length of  $2^{31}-1$  from a pulse pattern generator (PPG). The MZM is biased at quadrature point of the transmission curve to generate non-return-to-zero (NRZ) signals. The pump light is amplified by a high-power erbium-doped fiber amplifier (EDFA) followed by a variable optical attenuator (VOA) to adjust the pump power. The probe signal and the pump light are combined by a 3-dB coupler before injected into the device under test (DUT). The output signal is amplified using two cascaded EDFAs followed by two tunable band-pass filters (BPFs) to suppress the amplified spontaneous emission (ASE) noise. The BPFs are also utilized to

separate the probe signal from the pump light before fed into an oscilloscope to observe the eye diagrams. The bit-error-rate (BER) performances are measured by a photo detector (PD) followed by a BER tester (BERT).

The eye diagram of the input probe signal at  $IN_1$  is shown in Fig. 5a-I. The data rate is chosen to be 10 Gb/s. When the pump is off, the signal is output from  $OUT_1$ , which corresponds to the bar state. On the other hand, the signal is output from  $OUT_2$  when the pump is on, which corresponds to the cross state. The eye diagrams of the output signals at these two states are shown in Fig. 5a-II

and a-III, respectively. The threshold of the pump power for wavelength red shift is about 1 dBm (about  $-10$  dBm coupled into the DUT). The eye diagram in Fig. 5a-III is recorded when  $\lambda_1' = 1551.282$  nm in Fig. 3c is red shifted to  $\lambda_2' = 1551.516$  nm with a pump power of about 7.9 dBm. Figure 5b-I – b-III present the eye diagrams of the input probe signal at  $IN_2$ , the output signal at  $OUT_2$  when pump-off, and the output signal at  $OUT_1$  when pump-on, respectively. The data rate is chosen to be 12.5 Gb/s. The measured BER curves with signals input from  $IN_1$  and  $IN_2$  are shown in Fig. 5c and d, respectively. Compared

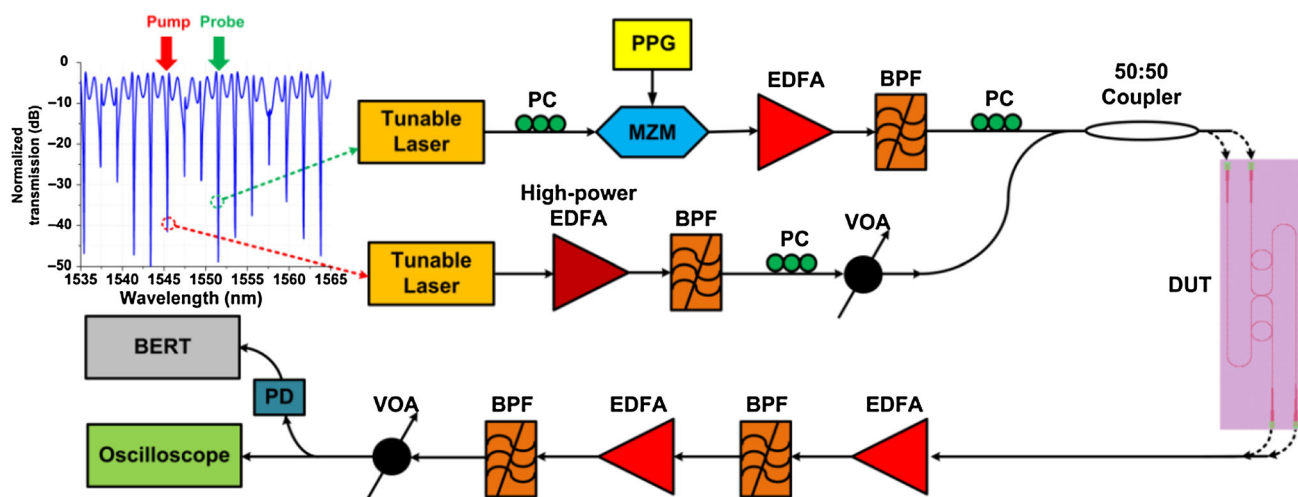


**Fig. 4** (Color online) Experimental setup for system demonstration of the switching function. The wavelengths of probe signal and pump light are set to 1551.516 and 1545.433 nm, respectively. *MZM* Mach-Zehnder modulator, *PC* polarization controller, *PPG* pulse pattern generator, *EDFA* erbium-doped fiber amplifier, *BPF* band pass filter, *VOA* variable optical attenuator, *DUT* device under test, *PD* photo detector, *BERT* bit-error-rate tester

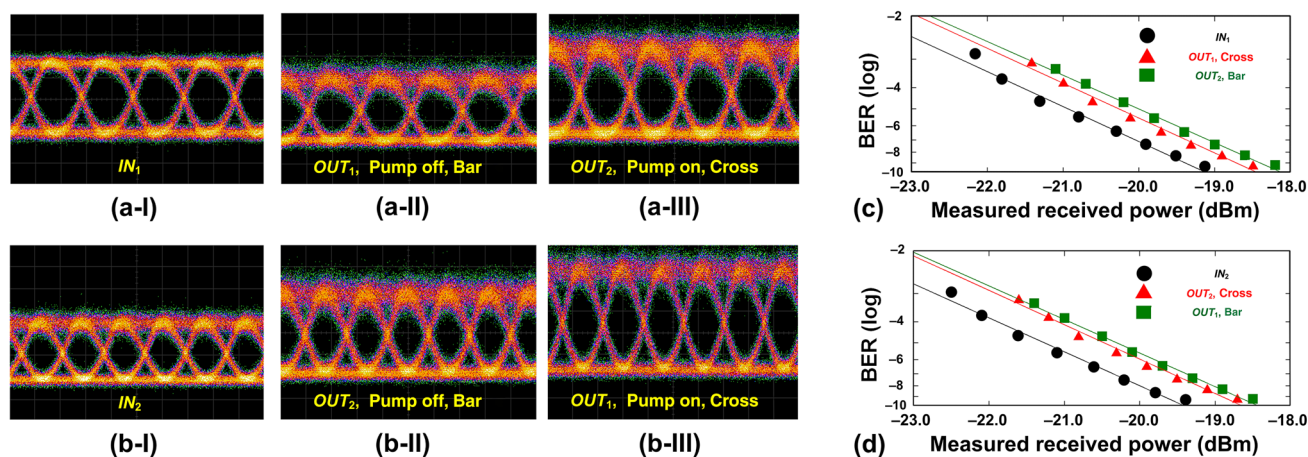


**Fig. 5** (Color online) Eye diagrams and BER performances. (a-I)–(a-III) Eye diagrams of input probe signal at  $IN_1$ , output signal at  $OUT_1$  when pump-off, and output signal at  $OUT_2$  when pump-on, respectively; (b-I)–(b-III) Eye diagrams of input probe signal at  $IN_2$ , output signal at  $OUT_2$  when pump-off, and output signal at  $OUT_1$  when pump-on, respectively; (c) and (d) Experimentally measured BER curves at cross/bar state with signals input from  $IN_1$  and  $IN_2$ , respectively

with the BER performances of the input probe signals, the output signals experience about 0.8-dB penalty at bar state and about 1.0-dB penalty at cross state.

### 5 Testing of the switching speed based on free carrier effect in silicon

We use the experimental setup shown in Fig. 6 to test switching speed of the fabricated device based on silicon free carrier effect. The wavelength of the probe light is set at  $\lambda_1 = 1551.282$  nm in Fig. 3b, and the wavelength of the pump signal sits at an adjacent resonance wavelength of 1548.585 nm in the measured transmission spectrum from  $IN_1$  to  $OUT_2$ , as shown in Fig. 6. When the input pump signal is bit ‘1’, there are free carriers generated in the silicon device, thus leading to blue shift of the transmission spectra. If  $\lambda_2 = 1551.516$  nm is blue shifted to  $\lambda_1 = 1551.282$  nm, the switching unit changes from cross state to bar state. On the other hand, the transmission spectra of the four-port silicon device are not shifted when the input pump signal is bit ‘0’ since there are no free carriers generated [22]. As a result, the bit pattern of the

pump signal is converted to the probe light. After separated from the pump signal by the BPFs after the DUT, the probe signal is fed into the oscilloscope for observation.

The experimentally observed temporal waveforms of 1 Gb/s input pump signal at  $IN_1$  and the converted output probe signal at  $OUT_1$  are shown in Fig. 7a and b, respectively. The power of the input pump signal and the probe light are about 7.2 dBm and about  $-5$  dBm, respectively. Although the pump power is above the threshold for wavelength red shift, there is not enough time for thermal accumulation since the bit rate of the input pump signal is on the order of Gb/s. As a result, one can observe the bit pattern converted to the probe light caused by free carrier effect. The available switching speed is mainly limited by the free-carrier lifetime in silicon. For intrinsic silicon photonic waveguides that are designed to be single mode at 1550 nm, the free-carrier lifetime is approximately about 500 ps [23], which corresponds to a minimum switching time of about 500 ps. The free-carrier lifetime can be greatly reduced by using a reversed-biased *p-i-n* junction or by ion implantation [24–26]. The minimum switching time of silicon microring-resonator-based switching unit with oxygen implanted can reach 25 ps [26].

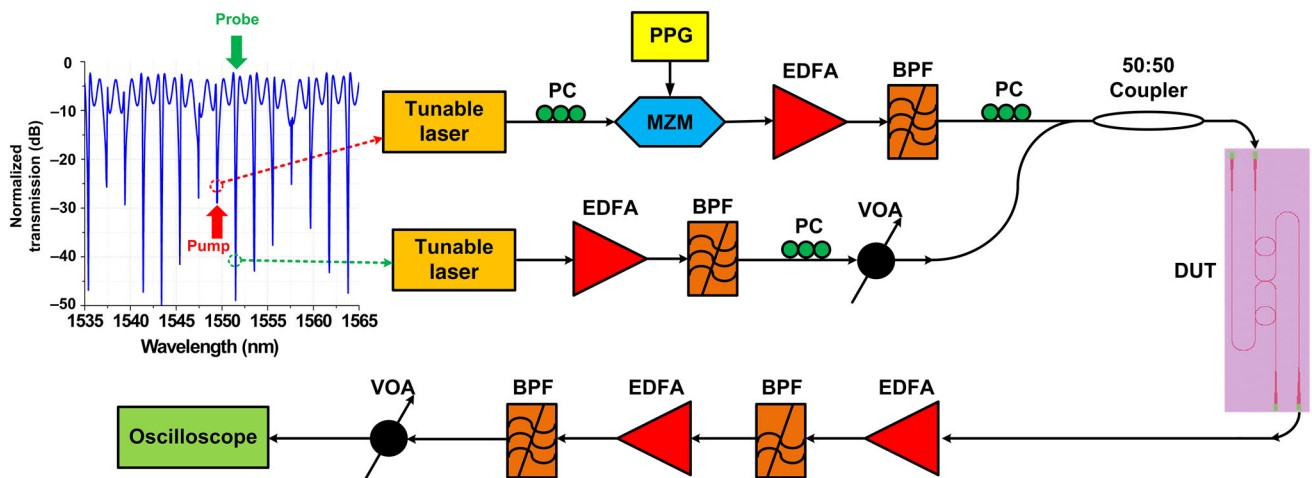


**Fig. 6** (Color online) Experimental setup for testing of switching speed based on silicon free carrier effect. The wavelengths of probe light and pump signal are set to 1551.282 and 1548.585 nm, respectively

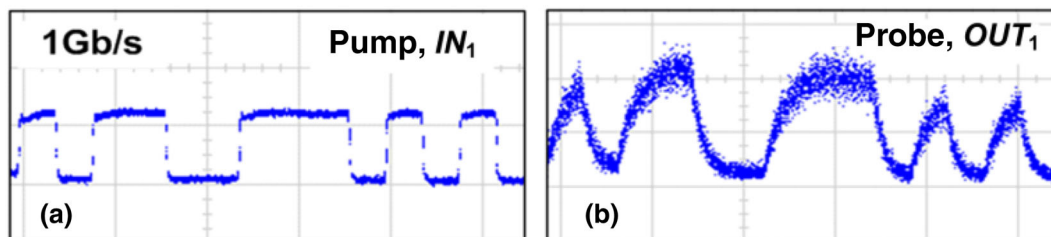


**Fig. 7** (Color online) Experimental results for the testing of switching speed based on silicon free carrier effect. **a** Temporal waveform of 1 Gb/s input pump signal at  $IN_1$ ; **b** Temporal waveform of 1 Gb/s output probe signal at  $OUT_1$

## 6 Conclusions

In conclusion, we have proposed and experimentally demonstrated an on-chip  $2 \times 2$  Benes switching unit based on two nested silicon MRRs with high ERs of about 44.7/38.0 dB and low crosstalk values of about  $-37.5/-45.2$  dB at cross/bar states. The effectiveness of the fabricated device is verified by system experiments with 10 and 12.5 Gb/s NRZ signals. Switching time of about 1 ns based on silicon free carrier effect is also experimentally demonstrated. The proposed device provides a way to improve the performances of ERs and crosstalks for switching nodes in optical NoCs, which could be helpful to the implementation of high-performance CMPs.

**Acknowledgments** This work was supported in part by the National Natural Science Foundation of China (61125504 and 61235007), in part by MoE Grant (20110073110012), and in part by Minhang Talent Program.

## References

1. Beausoleil RG, Kuekes PJ, Snider GS et al (2008) Nanoelectronic and nanophotonic interconnect. *Proc IEEE* 96:230–247
2. Shacham A, Bergman K, Carloni LP (2008) Photonic networks-on-chip for future generations of chip multiprocessors. *IEEE Trans Comput* 57:1246–1260
3. Biberman A, Bergman K (2008) Optical interconnection networks for high-performance computing systems. *Rep Prog Phys* 75:1–15
4. Miller DA (2009) Device requirements for optical interconnects to silicon chips. *Proc IEEE* 97:1166–1185
5. Haurylau M, Chen G, Chen H et al (2006) On-chip optical interconnect roadmap: challenges and critical directions. *IEEE J Sel Top Quantum Electron* 12:1699–1705
6. Ji RQ, Yang L, Zhang L et al (2011) Five-port optical router for photonic networks-on-chip. *Opt Express* 19:20258–20268
7. Li X, Xiao X, Xu H et al (2013) Mach-Zehnder-based five-port silicon router for optical interconnects. *Opt Lett* 38:1703–1705
8. Yang M, Green WM, Assefa S et al (2011) Non-blocking  $4 \times 4$  electro-optic silicon switch for on-chip photonic networks. *Opt Express* 19:47–54
9. Dong P, Preble SF, Lipson M (2007) All-optical compact silicon comb switch. *Opt Express* 15:9600–9605
10. Zhou L, Poon AW (2007) Electrically reconfigurable silicon microring resonator-based filter with wave-guide-coupled feedback. *Opt Express* 15:9194–9204
11. Xu Q, Schmidt B, Pradhan S et al (2005) Micrometer-scale silicon electro-optic modulator. *Nature* 435:325–327
12. Assefa S, Xia FN, Vlasov YA (2010) Reinventing germanium avalanche photodetector for nanophotonic on-chip optical interconnects. *Nature* 464:80–84
13. Bianco A, Cuda D, Garrich M et al (2012) Optical interconnection networks based on microring resonators. *J Opt Netw* 4:546–556
14. Lee BG, Biberman A, Sherwood-Droz A et al. (2008) High-speed  $2 \times 2$  switch for multi-wavelength message routing in on-chip silicon photonic networks. In: *Proceedings of the 34th European Conference on Optical Communication*, Sept 21–25, Brussels, Belgium
15. Yuen PH, Chen LK (2013) Optimization of microring-based interconnection by leveraging the asymmetric behaviors of switching elements. *J Lightw Technol* 31:1585–1591
16. Small BA, Lee BG, Bergman K et al (2007) Multiple-wavelength integrated photonic networks based on microring resonator devices. *J Opt Netw* 6:112–120
17. Bianco A, Cuda D, Gaudino R et al (2010) Scalability of optical interconnects based on microring resonators. *IEEE Photon Technol Lett* 22:1081–1083
18. Wu JY, Cao P, Hu XF et al (2013) Nested configuration of silicon microring resonator with multiple coupling regimes. *IEEE Photon Technol Lett* 25:580–583
19. Yariv A (2002) Critical coupling and its control in optical waveguide-ring resonator systems. *IEEE Photon Technol Lett* 14:483–485
20. Teng J, Dumon P, Bogaerts W et al (2009) Athermal silicon-on-insulator ring resonators by overlaying a polymer cladding on narrowed waveguides. *Opt Express* 17:14627–14633
21. Liu FF, Li Q, Zhang ZY et al (2008) Optically tunable delay line in silicon microring resonator based on thermal nonlinear effect. *IEEE J Sel Top Quantum Electron* 14:706–712
22. Li Q, Zhang ZY, Liu FF et al (2008) Dense wavelength conversion and multicasting in a resonance-split silicon microring. *Appl Phys Lett* 93:1–3
23. Almeida V, Barrios C, Panepucci R et al (2004) All-optical control of light on a silicon chip. *Nature* 431:1081–1084
24. Preble SF, Xu QF, Schmidt BS et al (2005) Ultrafast all-optical modulation on a silicon chip. *Opt Lett* 30:2891–2893
25. Först M, Niehusmann J, Plötzting T et al (2007) High-speed all-optical switching in ion-implanted silicon-on-insulator microring resonators. *Opt Lett* 32:2046–2048
26. Waldow M, Plötzting T, Gottheil M et al (2008) 25 ps all-optical switching in oxygen implanted silicon-on-insulator microring resonator. *Opt Express* 16:7693–7702